

Absorption related velocity dispersion below a possible gas hydrate geobody

Ian F. Jones

ION GX Technology, 1st Floor, Integra House Vicarage Rd., Egham Egham Surrey TW20 9JZ, United Kingdom

Received December 2011, revision accepted June 2012

ABSTRACT

Velocity dispersion is not usually a problem in surface seismic data processing, as the seismic bandwidth is relatively narrow and thus for most Q values, dispersive effects are not noticeable. However, for highly absorptive bodies, such as the overpressured free gas accumulations associated with some gas hydrates or high-porosity normally pressured gas sands, dispersive effects may be seen. In this work I analyse one such data set from the offshore north-east coast of India. I demonstrate that the effect is measurable and that compensating for it in either data processing or migration can improve the wavelet character, as well as delivering an estimate of the effective Q values in the associated geobody. I also raise the question as to whether velocities derived using low-frequency waveform inversion over such dispersive geobodies are wholly appropriate for migration of full seismic-bandwidth data.

Key words: Dispersion correction, Full-waveform inversion, Gas hydrate, Overpressure, Velocity dispersion.

INTRODUCTION

The initial motivation for this study came from the concern that velocities derived from full-waveform inversion (FWI) might not be wholly appropriate for migration of seismic data within the typical seismic bandwidth. Recent developments in tomographic inversion using the full waveform of the seismic data have proved successful in estimating the velocity distribution in small-scale near-surface low-velocity anomalies, such as those associated with gas accumulation. However, many of the techniques being used rely on the lowest frequencies present in the recorded seismic data. The question then arises as to whether the velocity estimated from such low frequencies will be appropriate for imaging full-bandwidth data where the dominant frequency may be several times that of those used in the inversion. Remember that although dispersive effects will mostly be negligible for surface seismic data, the one place they might be of influence will

be in absorptive low-velocity anomalous zones, which are prime candidates for the use of waveform inversion, which in turn may rely on the assumption that velocities estimated from low frequencies are valid for migration over the full data bandwidth. With the motivation to assess these questions in mind, here I attempt to assess whether velocity dispersion is significant enough to bias FWI velocity estimation for imaging below small-scale velocity anomalies. In the part of the study reported here, only the assessment of dispersive effects is considered.

The data in the study are from a deep water offshore area from eastern India (courtesy of Reliance Industries), discussed in two recent papers by Fruehn *et al.* (2008) and Smith *et al.* (2008). Possible gas hydrate formations form a potential trapping mechanism for free gas accumulation, which may become overpressured, constituting a geohazard. In order to obtain a good depth image below such low-velocity geobodies, their velocity structure must be adequately incorporated into the velocity-depth model. A commercial 3D preSDM project conducted in 2007–2008, covering some 2300 km², used high-resolution hybrid-gridded tomography (Jones,

*E-mail: ian.jones@iongeo.com

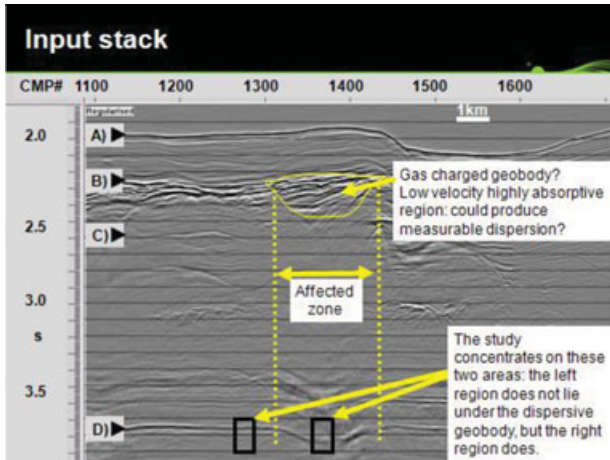


Figure 1 Data in the study area showing a low-velocity geobody and associated underlying push-down and dimming.

Sugrue and Hardy 2007) to delineate the gas-charged geobodies and update the velocity model so as to remove push-down effects below these geobodies.

Figure 1 shows an unmigrated stack of the data under consideration: the sequence of flat lying events with arrival times between 3400–3900 ms shows a severe push-down effect in the centre of the section (between CMPs 1300–1450). These events are at a depth of approximately 3200 m. Events below about 2500 ms are dimmed in this region, perhaps due to absorptive effects in the overlying highly reflective geobody. For data in parts of this region of offshore India, it is known that a gas hydrate layer is present (e.g., Chaudhuri *et al.* 2002); these hydrate layers have been drilled and core-sampled in some studies (e.g., Riedel, Willoughby and Chopra 2010). The hydrate layer sits about 200 m below the sea-bed, in waters of depth greater than about 400 m and appears as a relatively bright reflector which sub-parallel the sea-bed and can cross-cut the sedimentary layers. Because of this, the hydrate layer is sometimes referred to as a bottom-simulating reflector (BSR). If gas is leaking from an underlying reservoir, or being evolved from localized biogenic activity or hydrate dissociation, then free gas can accumulate below the frozen gas hydrate cap. In this case a geohazard can develop if the trapped gas becomes overpressured.

Figure 2 shows the initial smooth velocity model superimposed on a preliminary 3D preSDM image of the data, with the geobody location indicated (upper image). Diffraction energy is collapsed by migration but the push-down remains, as the geobody's low-velocity effect is not yet accounted for. After two iterations of 3D tomography, the low-velocity geobody

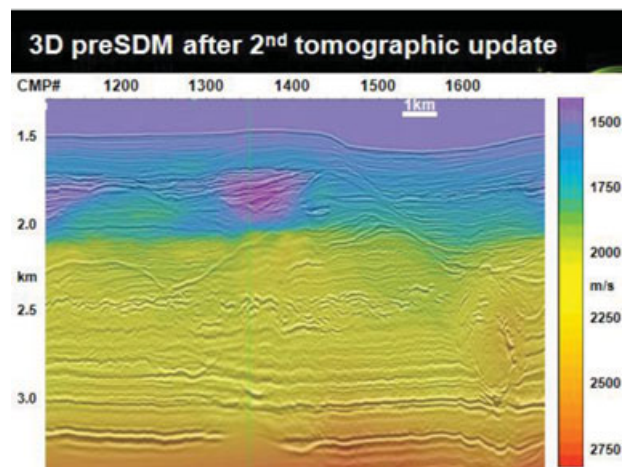
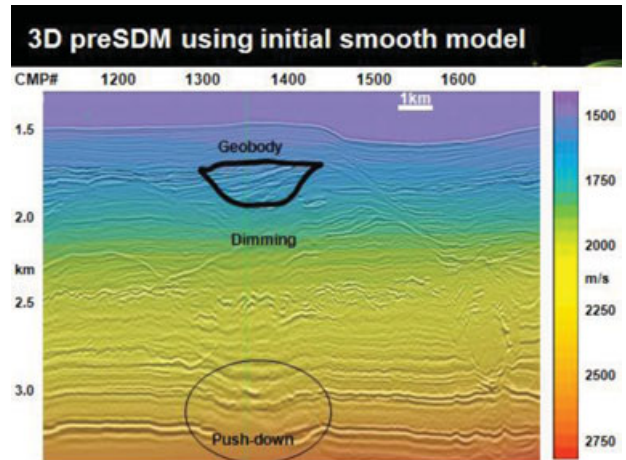


Figure 2 Top: initial 3D preSDM using the smooth velocity model. Bottom: 3D preSDM after 2nd iteration of tomographic update, including geobody velocity feature. The respective interval velocity models are superimposed.

is incorporated into the model, so the push-down is mostly resolved (lower image).

GEOBODY AVERAGE VELOCITY ESTIMATION

The background velocity was estimated during the Pre-Stack Depth Migration (PreSDM) iterative velocity model update and the velocity associated with the low-velocity geobody was estimated in three different ways:

Method 1) conventional preSDM tomographic inversion of the full-bandwidth data from the 'commercial' imaging project

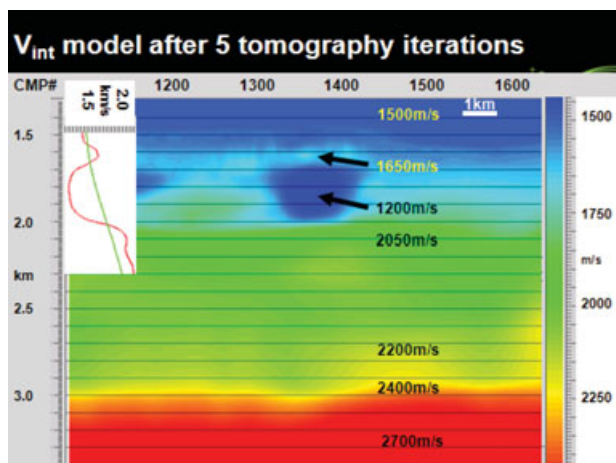


Figure 3 Interval velocity profile after five iterations of tomographic update, used for the final 3D preSDM. The inset in the upper-left corner shows a velocity profile extracted through the geobody, clearly indicating the increase in velocity at the top of the body.

Method 2) push-down analysis of the near-offset section from the unmigrated full-bandwidth data

Method 3) velocity-spectra analysis of the unmigrated full-bandwidth data

Method 1) Figure 3 shows the interval velocity model obtained after five iterations of 3D hybrid gridded ray-based tomography. At the level of the bright geobody (times 2200–2500 ms, roughly corresponding to depths 1700–1950 m), the interval velocity profile from the preSDM tomographic model shows a characteristic increase in velocity at the top of the hydrate layer, overlying a significantly lower velocity region (with interval velocity perhaps between 1200–1400 m/s) set in a background velocity of about 1750 m/s. These velocities were determined using preSDM CRP autopicking on a 50 m * 50 m picking grid, with 3D gridded tomographic inversion using a cell size of 500 m * 500 m * 100 m (Fruehn *et al.* 2008). A pure methane hydrate layer has a P-wave velocity of about 3730 m/s but even a slight gas saturation (>2%) in the underlying sediment will cause a significant reduction in velocity compared to the surrounding sediment velocity, typically in the range of about 1540–2200 m/s (Minshull, Singh and Westbrook 1994; Collett and Dallimore 2002; Reister 2003). In the inset in the upper left of Fig. 3, we see a velocity profile extracted through the geobody (the red line) indicating an increase in velocity to about 1700 m/s at the top of the geobody, with a drop to about 1300 m/s below this (the green line shows the background velocity trend).

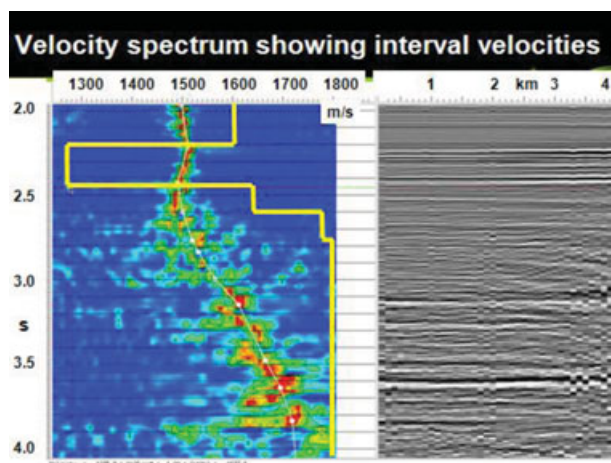


Figure 4 Velocity analysis and NMO corrected CMP gather over the geobody, using up to 4 km offsets, indicating unusually low-interval velocity

Method 2) Using a simple push-down analysis of the deeper events (at 3200 m, or about 3800 ms) measured from the near-trace offset section of unmigrated full-bandwidth data and assuming that the geobody is 200 m thick (sitting between depths 1700–1900 m), set in a background velocity of 1750 m/s, with an average deeper velocity of about 2000 m/s, then the observed time push-down of 80 ms twt (two-way time) implies an interval velocity in the geobody of about 1350 m/s. (Push-down or pull-up analysis simply estimates the interval velocity variation required to produce an image distortion, under the assumption that the horizon in question should actually be flat-lying.)

Method 3) Conventional velocity analysis of the raw full-bandwidth data centred over the geobody suggests an interval velocity of about 1270 m/s, although this estimate will be corrupted due to raypath distortion within the CMP ray-bundle: the low-velocity anomaly is about 2.5 km wide, whereas the acquisition cable is 6 km long, therefore the moveout behaviour in the CMP gathers will not be hyperbolic, introducing a bias into such a velocity estimation. Figure 4 shows the velocity spectrum with instantaneous Dix interval velocity estimates superimposed.

DISPERSIVE EFFECTS

Attempts to measure absorption related dispersion on conventional surface streamer marine seismic data are notoriously difficult, due to the almost negligible effect of velocity dispersion in the measured bandwidth at typical seismic frequencies. If dispersion was found, it would mostly relate to the lowest

frequencies in the signal compared to the highest. Such effects were addressed in the early days of vibroseis processing so as to compensate for dispersive effects prior to correlation (e.g., the ‘CombiSweep’ technique of Werner and Kray 1979).

In this study, using marine streamer seismic data, I attempt to measure dispersive effects associated with what was thought to be a gas-charged geobody underlying a gas hydrate cap where we have low-seismic velocities and significant absorption effects. However, it should be noted that from seismic arrival time data alone, it is difficult to distinguish between an overpressured gas-sand geobody and a high-porosity normally pressured gas-charged sand-clay geobody, as both can have anomalously low velocities compared to the surrounding sediments. The actual nature of this geobody does not detract from the general thrust of the analysis, as it is clearly a low-velocity absorptive body, even if it is not gas charged. The low velocity nature of this geobody is indicated by the push-down in the deeper layers and the significant dimming below it is indicative of strong absorption, as characterized by the low Q values measured using spectral-ratio analysis (discussed below). Analysis of amplitude spectra computed along four horizons (shown in Fig. 5) also indicates this loss of energy: smoothed spectra were computed in short windows centred on these horizons along: A) the sea-bed, B) the top of the hydrate layer, C) a weak event at ~ 2.6 s twt corresponding to the depth of the base of the low-velocity geobody and D) along a strong deep reflector.

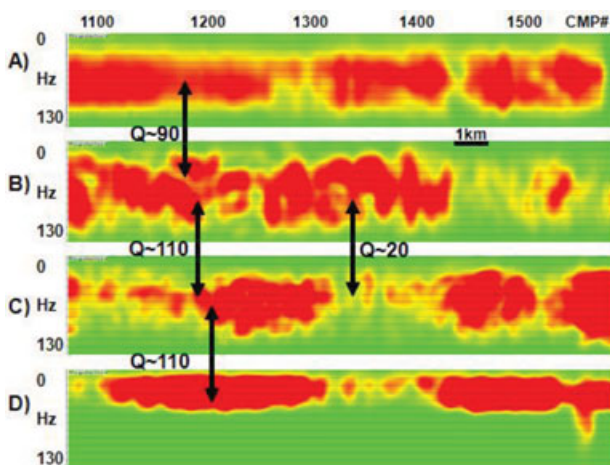


Figure 5 Amplitude spectra for traces along four horizons (positions indicated on Fig. 1): A) the sea-bed reflector, B) top hydrate, C) an event corresponding to the depth of the base geobody at about 2.6 s twt, D) strong deep event at about 3.8 s twt. Spectra are normalized for each individual horizon.

Using spectral ratio analysis (Jacobson *et al.* 1981), an estimate of effective Q was made between these four horizons. The effective Q value between the sea-bed and the top hydrate is about 90, in the deeper sediments it rises to over 110 and within the geobody it seems to be between 15–20 (depending on which particular small window is used), compared to a value of about 110 to the sides of the geobody.

These effective Q estimates relied on very heavy smoothing and averaging of spectra and are not directly measuring evidence of dispersive effects. Additionally, there will also be a scattering as well as an absorptive component to the measured amplitude loss. In an attempt to obtain consistent and cross-validated estimates of actual dispersion, two approaches were employed using data in several narrow frequency bands:

- 1) near-trace arrival times were measured as a function of centre frequency on both raw and migrated data
- 2) RMS velocities were measured from velocity spectra computed for the seismic data in various frequency bands.

ARRIVAL-TIME ANALYSIS

Figure 6 shows a zoom of the stacked data from Fig. 1, indicating two small windows to be used for analysis: one outside and one inside the affected zone. For a series of narrow band-pass filters, I measured the arrival time of the near-trace event (without NMO correction, so as to avoid any possible wavelet distortion) for the deep reflector in the unaffected and affected zones. Within the affected zone, we observe a consistent and increasing delay of the arrival as we lower the band-pass

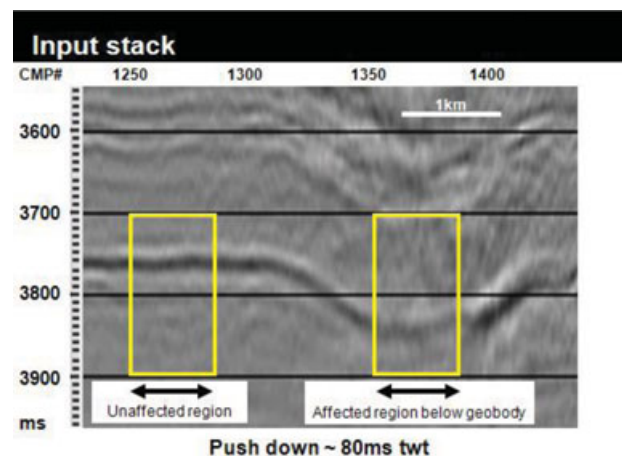


Figure 6 Zoom on the study areas: the reflector at about 3760 ms twt on the left of the figure is not influenced by the overlying geobody, whereas the segment to the right shows apparent push-down and loss of signal character.

frequency, which is consistent with what would be expected for dispersive body waves, in that the velocity will decrease with decreasing frequency (Futterman 1962).

These two regions were analysed for both the unmigrated near-trace data (200–300 m offsets, without NMO correction) and the near-trace preSDM data. For the purposes of this study, a single 2D line of data was analysed, hence the migrations shown are from 2D preSDM, as opposed to the 3D preSDM data considered in the commercial project (Fruehn *et al.* 2008; Smith *et al.* 2008).

In the study, I used several different zero-phase band-pass widths and shapes, both implemented in the time and frequency domain, all of which lead to comparable conclusions. Figure 7 compares the near-trace display of unmigrated data for these two regions with interpretations of the horizon arrival time (central peak) for three band-pass filtered data sets and the full-bandwidth data with the horizon interpretations superimposed.

The band-pass filters were selected so as to divide the usable signal into smoothly tapered overlapping zones. However, the

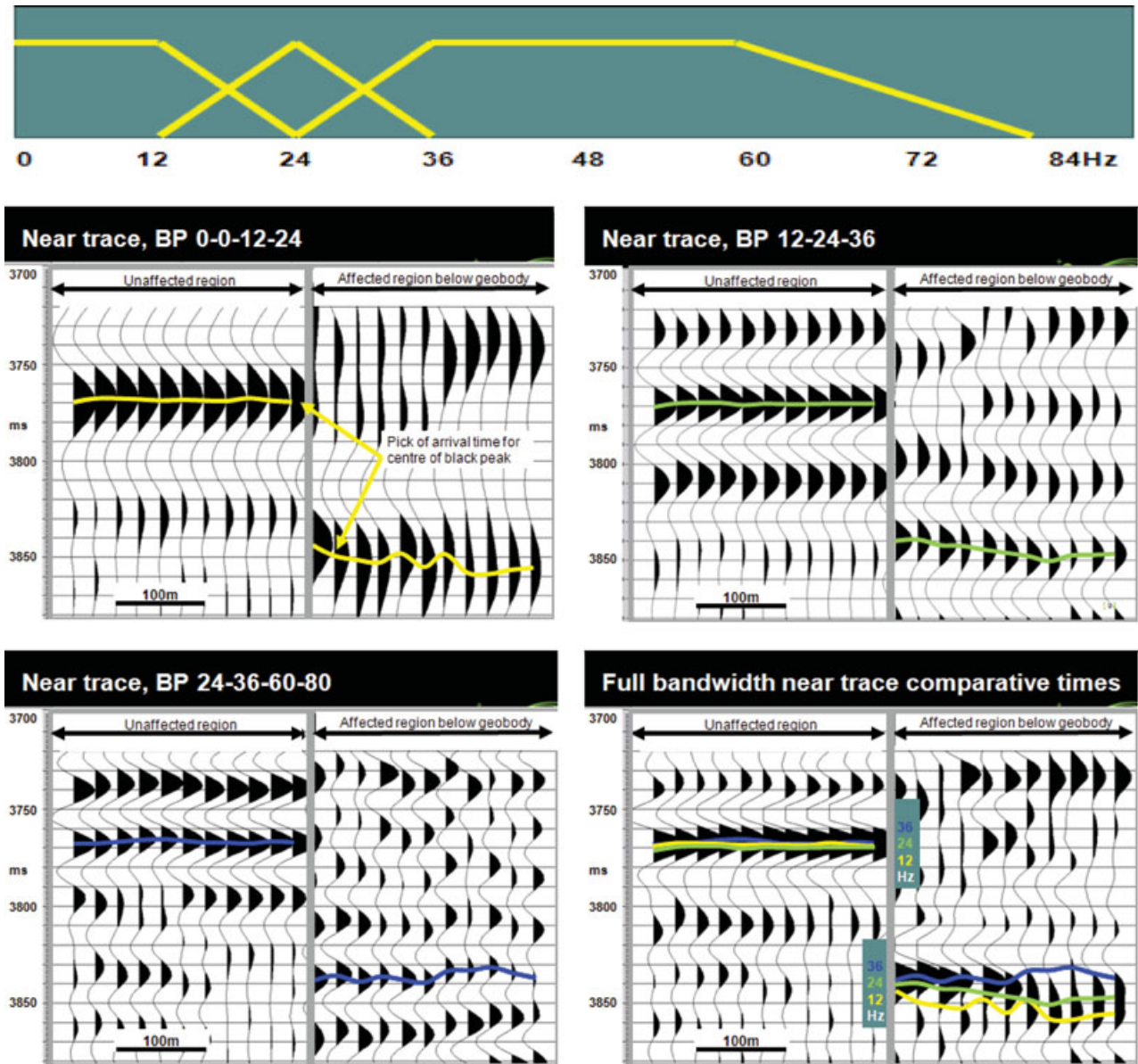


Figure 7 Upper figure shows the band-pass filters used and the other figures show the arrival times picked for the central peak of the wavelet for various band-limited data sets. Lower-right image compares the three sets of picked arrival times superimposed on the full-bandwidth data.

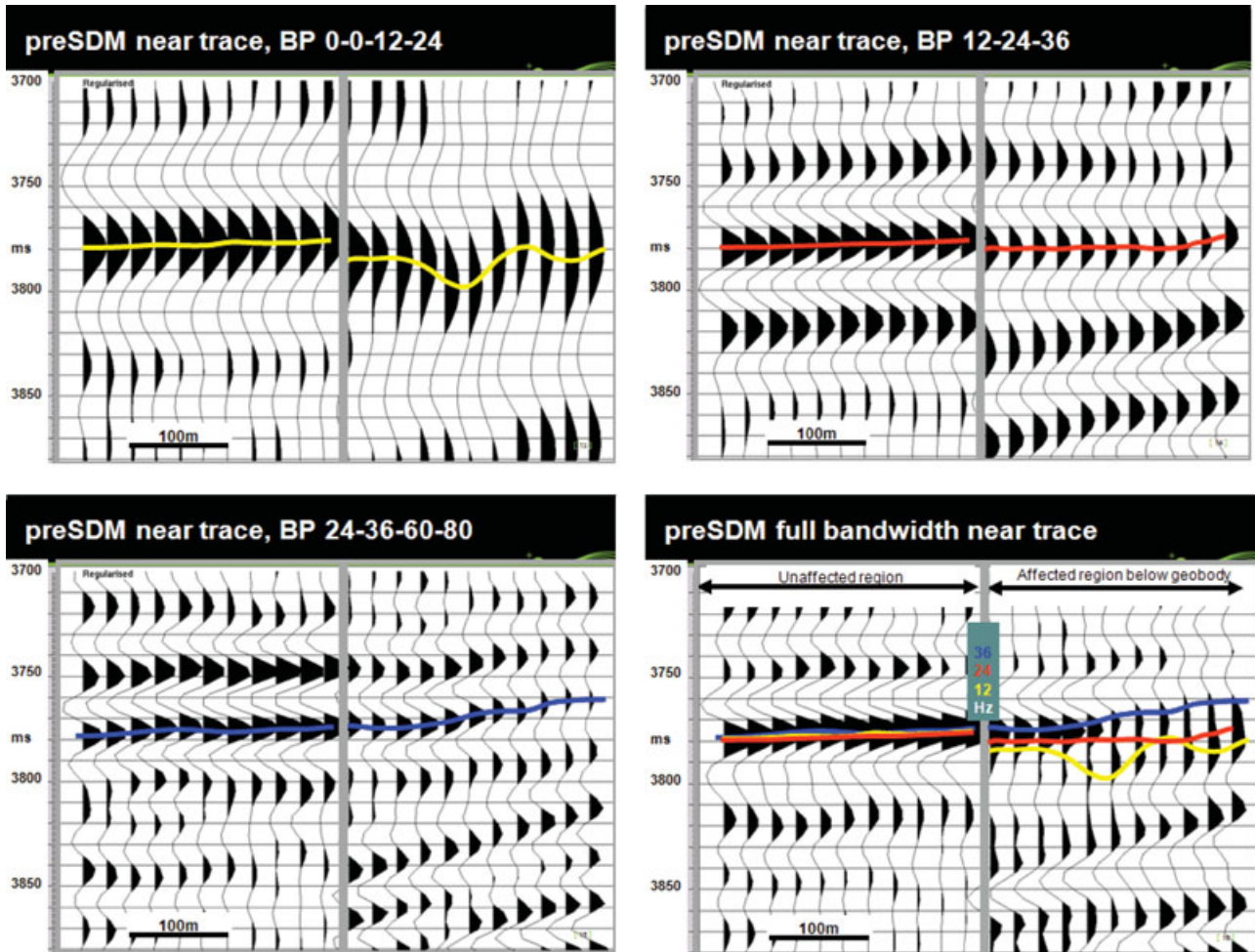


Figure 8 Data after preSDM and converted to time with a smooth model: arrival times picked for the central peak of wavelet for various band-limited data sets. Lower-right image compares the three sets of picked arrival times superimposed on the full-bandwidth data.

low-frequency filter extended fully-open to zero and the high-frequency filter extended to encompass the highest usable frequencies in the signal. The reason for this is that I later sum the filtered data so as to reconstruct the full-bandwidth signal. The filter characteristics are shown in Fig. 7. In Fig. 8, I compare the two regions as seen on the preSDM near trace (200–300 m offsets) converted back to time with a very smooth model in order to apply the filters, for the same selection of the three band-pass filters.

DISPERSION ANALYSIS

For the affected zone, I measured a two-way traveltime difference of between 10–20 ms on the picked time of the horizon, between the first and third (i.e., the ~12 Hz and ~36 Hz centred) filter images and given that the measured velocity in the

200 m thick geobody is about 1450 m/s on average, then if we assume that this two-way time delay difference was accumulated solely in the geobody (in other words, the underlying sediments have a much higher Q value resulting in negligible dispersion), then we can infer that the slower low-frequency velocity would be about 1400 m/s

Starting with the Futterman (1962) relationship for a constant Q model (i.e., Q invariant with frequency) and using a Taylor expansion for the tangent term for small values of $1/Q$ (e.g., Liu, Anderson and Kanamori 1976; Sun, Milkereit and Schmitt 2009), then the approximate relationship for velocity change as a function of frequency is:

$$v(f_2)/v(f_1) = 1 + (1/\pi Q) \ln(f_2/f_1). \quad (1)$$

Using $f_1 = 12$ Hz, $f_2 = 36$ Hz, and solving for representative values of $v(f_2) = 1450$ m/s and $v(f_1) = 1400$ m/s gives

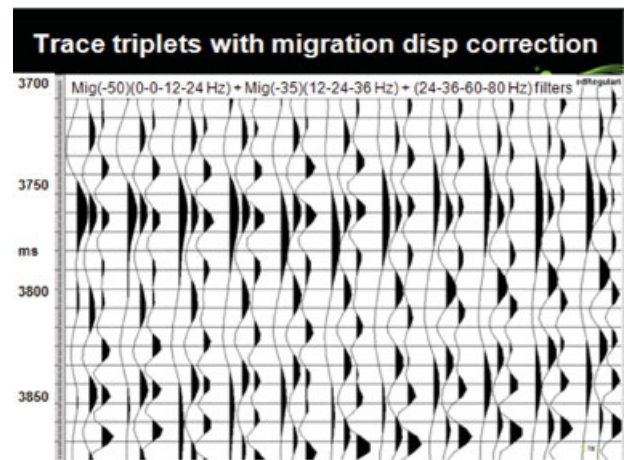
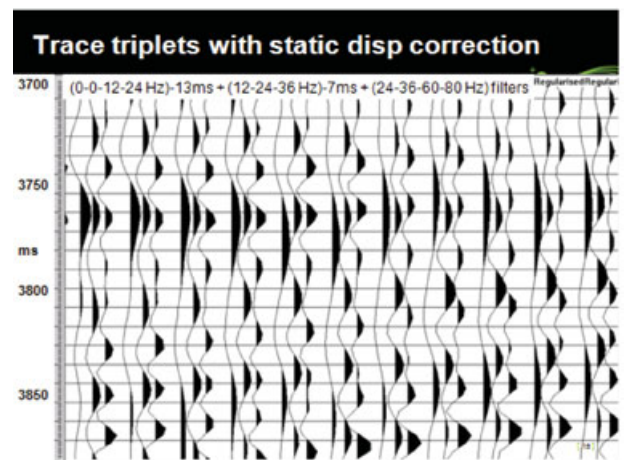
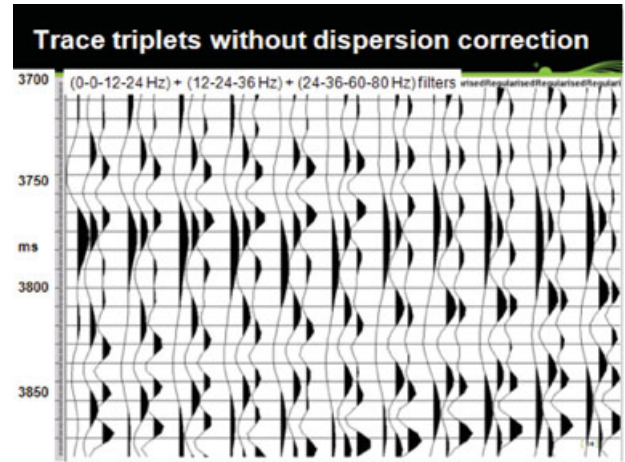
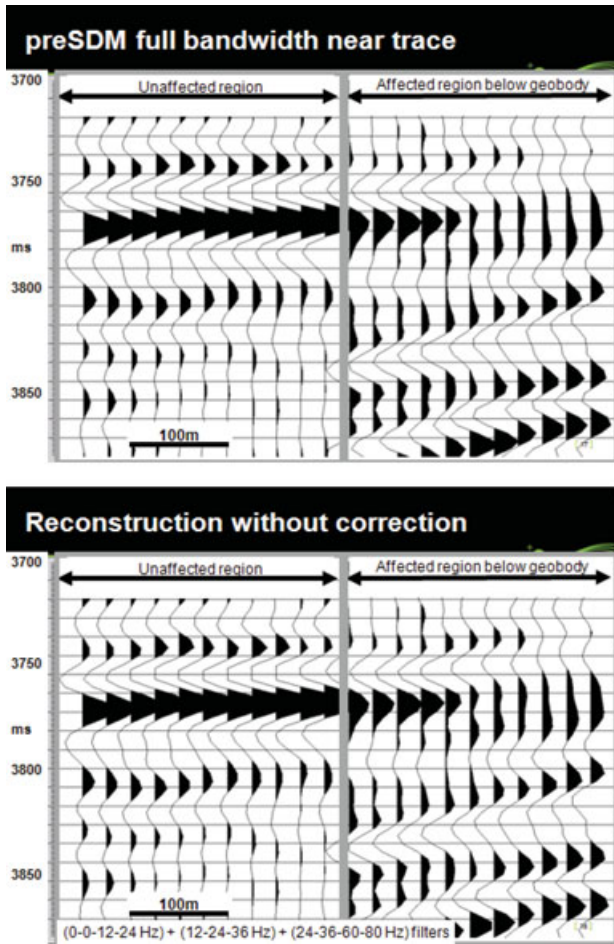


Figure 9 Top: migrated near-trace. Bottom: summation of the near-trace triplets after band-pass partitioning; no correction was applied – this image is a QC to ensure that a recombination of the partitioned data reproduces the input. (The data were converted to time with a smooth model following preSDM.)

$Q = 10$, which is at the low end of values described in the literature (e.g., Carcione and Helle 2002).

DISPERSION CORRECTION

Measuring and applying the static shifts required to align the waveform in the different bandwidths, gives us a first-order dispersion correction, applied to the data after migration. The high-frequency arrival is used as the reference and the other frequencies are adjusted to match its arrival time. Applying this correction gave a reasonable compression of the dispersed wavelet in the perturbed zone.

To verify that the band-pass data partitioning is correct and does not in itself modify the data significantly, I first sum the

Figure 10 Groups of three traces, corresponding to the three band-pass filters, for data within the affected zone. Top: the individual triplets migrated without dispersion correction. Middle: data after approximate static-shift correction. Bottom: migrations with dispersion correction. (The data were converted to time with a smooth model following preSDM.)

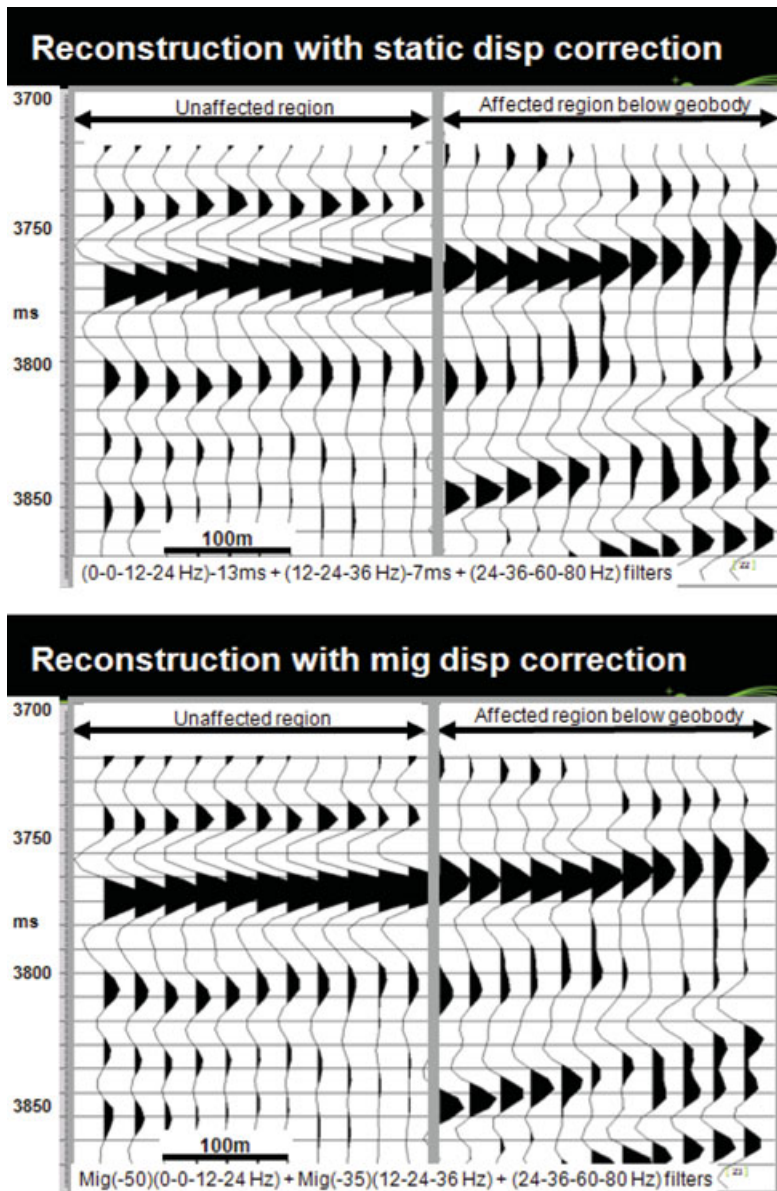


Figure 11 Summation of the trace triplets with dispersion correction, using (top) the static shift approach and (bottom) the migration approach. (The data were converted to time with a smooth model following preSDM.)

weighted band-passed traces without the dispersion correction to ensure that the input can be reconstructed. This QC step is shown in Fig. 9, comparing the migrated near trace, with the sum of the band-pass partitioned data.

As an alternative to using static shifts, I then migrated the different bandwidth data with a velocity model where the anomaly was adjusted so that its interval velocity changes as follows to accommodate the dispersion:

(24–36–60–80 Hz) uses the original velocity model

(12–24–36 Hz) has the anomaly velocity reduced by 35 m/s

(0–0–12–24 Hz) has the anomaly velocity reduced by 50 m/s

In this study, I did not modify the migration code to accommodate dispersion (Zhang, Zhang and Zhang 2010) but simply partitioned the data and migrated in various frequency bands with different velocity models (the models being locally scaled so as to compensate for the observed traveltimes delays), so as to demonstrate the dispersive effects and their compensation. The migrated results were then weighted and summed to give the dispersion correction. Figure 10 shows

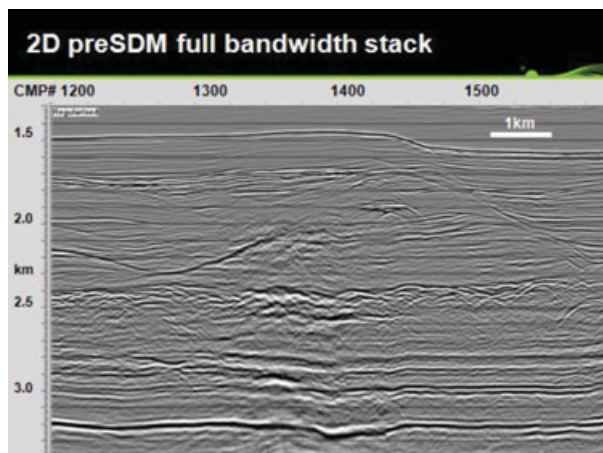


Figure 12 preSDM stack for offset range 0–3300 m.

the seismic traces in the perturbed zone, with each trace reproduced three times, once for each band-pass filter. Shown are these trace triplets without the corrections (top), with the static-shift approximate corrections (middle); and with the migration dispersion correction for frequency-dependent velocity in the migration (bottom). The wavelets are better aligned across the trace triplets after the migration dispersion correction.

Performing the reconstruction after dispersion correction for both the static shift and the migration approaches, produced the near-trace frequency partition summed sections shown in Fig. 11. A clear improvement in wavelet stationarity is evident, indicating that the frequency dependence of arrival times was removed reasonably well (compare to the uncorrected near-trace data in Fig. 9).

The preSDM stacked result for offset range 0–3300 m for the entire line is shown in Figs 12 and 13, without and with the migration dispersion correction, using the final interval velocity model. Overall the effect of the dispersion correction is not very noticeable on the stacked images but the wavelet phase on the deeper events is closer to zero. The residual moveout errors in the gathers following 2D preSDM probably smears the results a bit too much for these stacked sections to be of use. Performing the migration dispersion correction fully within a 3D preSDM algorithm (as demonstrated by Zhang *et al.* 2010) would be more a sensible approach to forming a corrected image.

VELOCITY ANALYSIS

A similar analysis was performed on velocity spectra for differing data bandwidths, to attempt to verify the conclusions using the offset kinematics. Using the full offset range

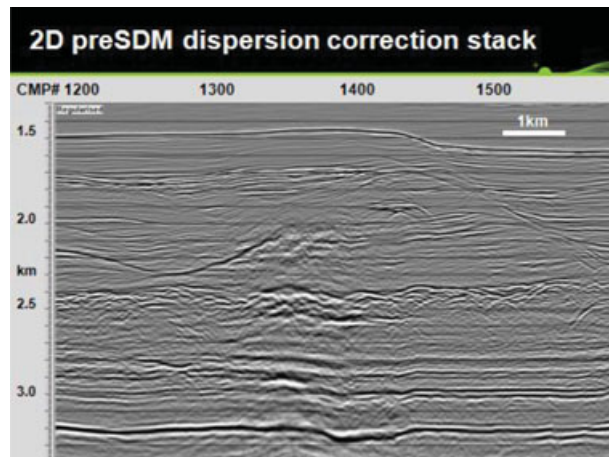


Figure 13 preSDM stack for offset range 0–3300 m for the dispersion corrected result.

(0–6 km) was influenced by higher order moveout effects, so I limited the offset range for velocity analysis to 0–4 km (Fig. 14).

Overall, the velocity analysis results are unconvincing, primarily due to the large error bars. However, I have included this analysis for completeness.

The band-passed data velocity analysis for four triangular filters is shown in Fig. 15. The CMP gather shown corresponds to the full-bandwidth gather shown in Fig. 14 (time window 3500–4000 ms; offsets 100–4000 m). These results are very tentative as the analysis is unreliable due to the very ‘ringy’ nature of the narrow band-limited spectra. However, the general trends observed in velocity with respect to frequency are consistent with the expected results for a dispersive medium.

Table 1 summarizes the results of the velocity analyses of the data in different bandwidths shown in Fig. 15: the error bars are the inherent uncertainties from the resolution analysis based on the maximum available offset (x_{\max}), peak frequency (F_c), arrival time (T_0) and average RMS velocity V_{rms} (Ashton *et al.* 1994; Jones 2010).

$$VRMS_{\text{error}} = T_0 V_{\text{rms}}^3 / (4F_c x_{\max}^2). \quad (2)$$

As expected for a dispersive medium, the arrival time of the reflection event decreases and the velocity increases with increasing frequency. However, the uncertainties on these estimates are probably too large for them to be considered meaningful.

Assessing what interval velocity anomaly in the shallow geobody must exist to create these observed RMS velocities at

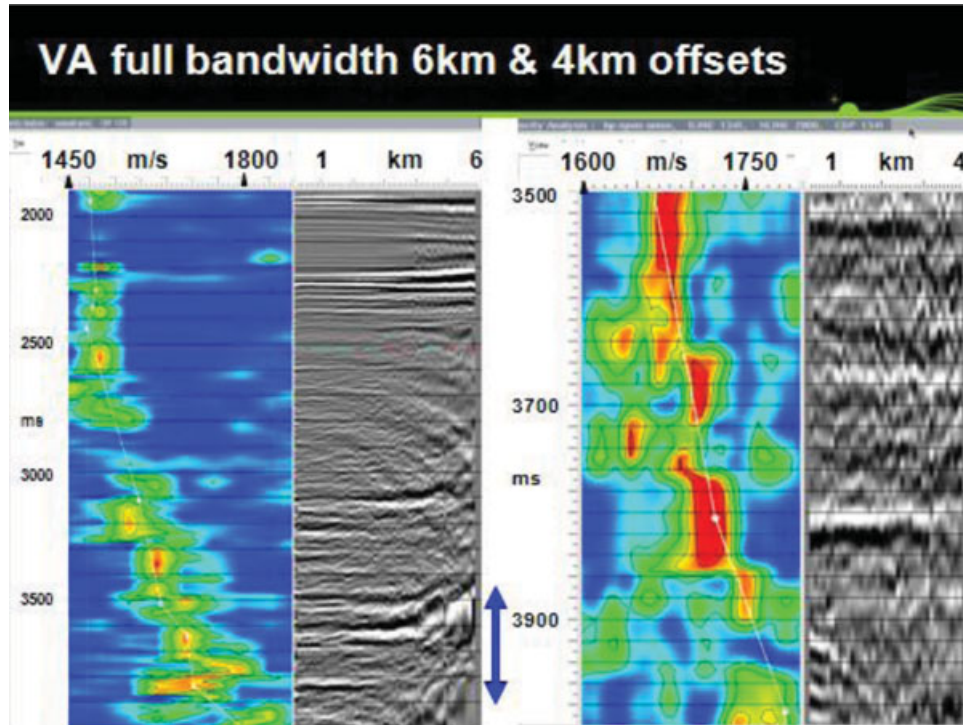


Figure 14 Left: velocity analysis and CMP gather for a 6 km cable. Right: zoom on the velocity spectrum and CMP gather for only a 4 km offset in the time window indicated by the blue arrow.

the deep horizon (at ~ 3830 ms) gives rise to the results shown in Fig. 16. In these calculations, I have made the assumption specified earlier in the delay-time calculations, that the geobody is 200 m thick sitting between a depth of 1700–1900 m, with neighbouring interval velocities of 1750 m/s and an underlying velocity of 2000 m/s.

The range of possibilities for the interval velocity in the shallow anomaly, between 1120–1300 m/s determined from simple Dix inversion of the measured RMS-stacking velocities, is consistent with the other estimates made in this study.

DISCUSSION

It should be noted that the conclusions drawn here are speculative in as much as the geobody under discussion resembles an overpressured free gas accumulation below a gas-hydrate cap but this is only inferred from the observed seismically derived properties and not characterized directly from well measurements. Developing overpressure needs a mechanism such as hydrate dissociation (e.g., Holtzman and Juanes 2011) or deeper reservoir seepage and from these seismic data

alone, it is unclear as to what mechanism, if any, is in play here.

High attenuation has previously been related to low-gas saturation (e.g., Walls *et al.* 2002) and low velocity in conjunction with high attenuation related to soft and overpressured sediments (e.g., Mavko 2005). Additionally, low velocity is also associated with high-porosity gas-charged but otherwise un-pressured, sand/shale sequences (Truman Holcombe, pers. com).

The anomalously low-interval velocity estimates look reasonable for an overpressured gas (Carcione *et al.* 2003) but without elastic impedance inversion with well-calibration, it is still uncertain as to what the geobody actually is. However, the manifestation of dispersion appears to be real, as the geobody is highly absorptive, even if it is not an overpressured zone. For the deep reflectors perturbed by the overlying absorptive region, interval velocity differences of about 3% were inferred between 12–36 Hz components of the data from the traveltime delay analysis and of about 2% from the (more error prone) velocity spectral analysis. These differences are similar to the results of Sun and Milkereit (2008) for a VSP study on the Mallik gas hydrate well.

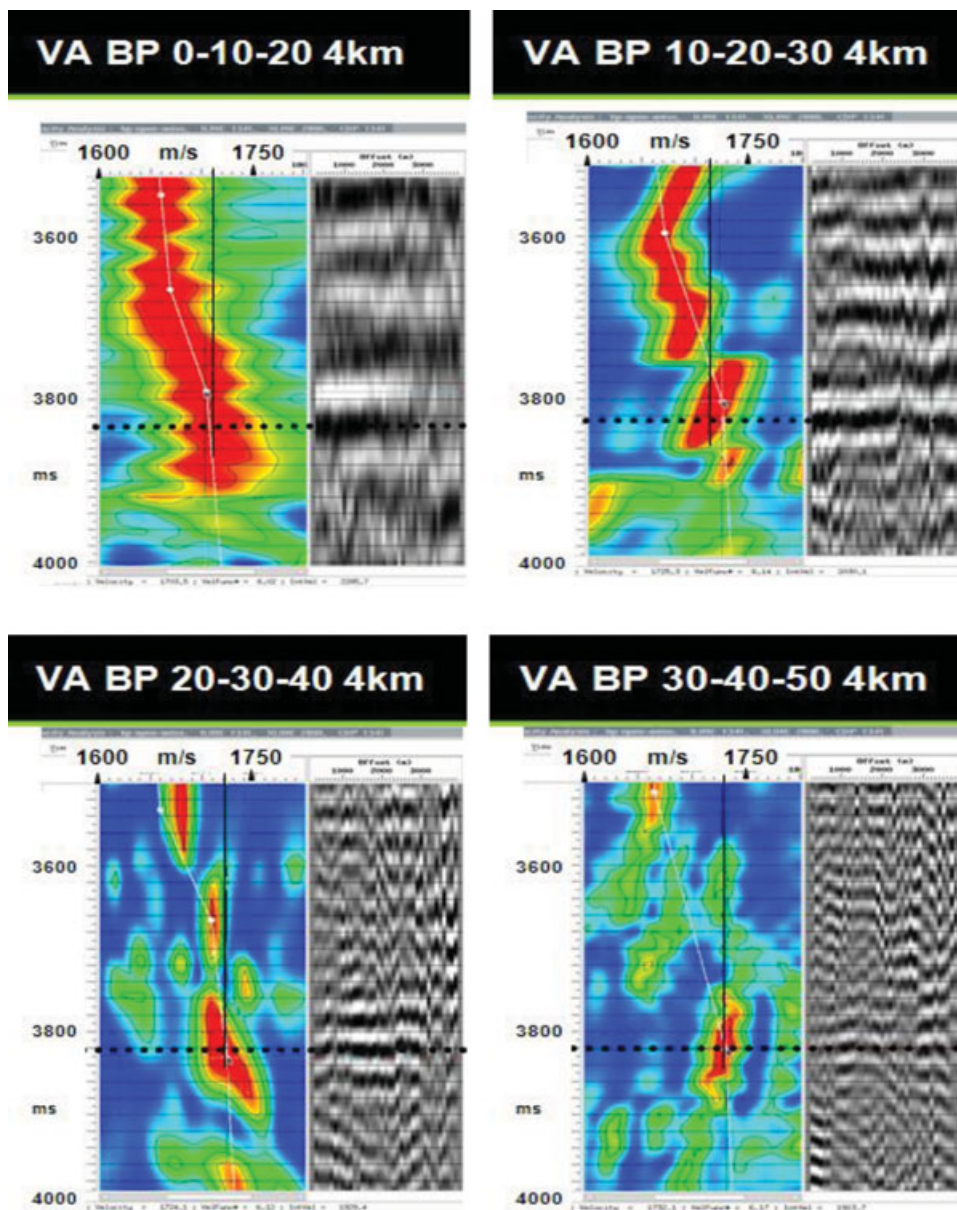


Figure 15 Velocity analysis for the deep event in different bandwidths, results summarized in Table 1.

Table 1 Velocity estimates as a function of bandwidth centre frequency, with intrinsic measurement error estimates. The triangular frequency bands used for the velocity analysis were: 0–10–20 Hz, 10–20–30 Hz, 20–30–40 Hz and 30–40–50 Hz.

Band F_c (Hz)	T_0 (ms)	V_{stacking} (m/s)
10	3832	1710 (± 30)
20	3828	1711 (± 15)
30	3822	1720 (± 10)
40	3820	1730 (± 7)

The estimated velocity dispersion over the recorded seismic bandwidth is perhaps significant enough for a migration velocity estimated from FWI to be measurably biased. An elegant solution to this problem is offered via use of visco-acoustic (Q) migration (e.g., Zhang *et al.* 2010).

ACKNOWLEDGEMENTS

My sincere thanks to Dr. Rabi Bastia, at Reliance Industries for permission to use the data for this study and to my

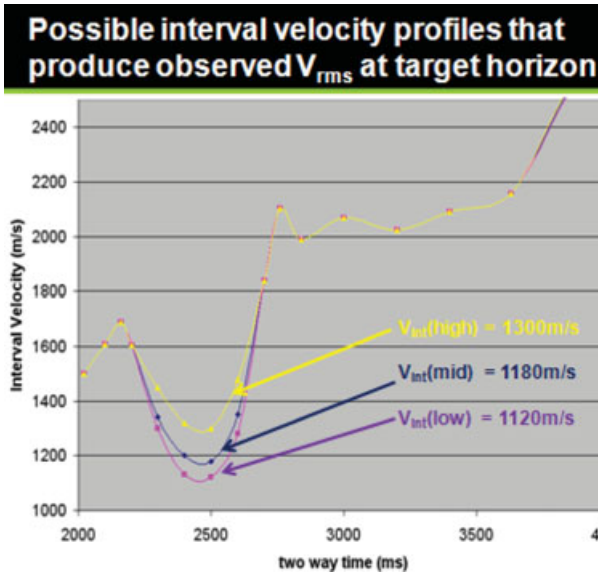


Figure 16 One possible set of solutions for the Dix interval velocity profiles that give rise to the observed RMS stacking velocities in the different bandwidths.

colleague Phil Smith at GXT for help with data preparation and to Mike Goodwin, Truman Holcombe, John Tinnin and Huub Douma for helpful suggestions with the work. Thanks to Professor Tim Minshull at the University of Southampton for some background material on gas hydrate behaviour. Thanks also to the reviewers whose feedback significantly improved the paper and to ION GX Technology for permission to publish this work.

REFERENCES

- Ashton C.P., Bacon B., Deplante C., Sinclair T. and Redekop G. 1994. 3D seismic survey design. *Oilfield Review*, April, 19–32.
- Carcione J.M. and Helle H.B. 2002. Rock Physics of Geopressure and Prediction of Abnormal Pore Fluid Pressure Using Seismic Data. *CSEG Recorder* V27, No. 7, 8–32.
- Carcione J.M., Helle H.B., Pham N.H. and Toverud T. 2003. Pore pressure estimation in reservoir rocks from seismic reflection data. *Geophysics* 68, No. 5, 1569–1579.
- Chaudhuri D., Lohani N., Chandra S. and Sathe A. 2002. AVO attributes of a bottom simulating reflector: East coast of India. 72nd SEG Meeting, Expanded Abstracts, 300–303.
- Collett T.S. and Dallimore S.R. 2002. Integrated Well Log and Reflection Seismic Analysis of Gas Hydrate Accumulations on Richards Island in the Mackenzie Delta, N.W.T., Canada. *CSEG Recorder* October, 2002, 28–40.
- Fruehn J.K., Jones I.F., Valler V., Sangvai P., Biswal A. and Mathur M. 2008. Resolving Near-Seabed Velocity Anomalies: Deep Water Offshore Eastern India. *Geophysics* 73, No. 5, VE235–VE241.
- Futterman W.I. 1962. Dispersive Body Waves. *Journal of Geophysical Research* 67, No. 13, 5279–5291.
- Holtzman R. and Juanes R. 2011. Thermodynamic and Hydrodynamic Constraints on Overpressure Caused By Hydrate Dissociation: A Pore-Scale Model. *Geophysical Research Letters* 38, L14308.
- Jacobson R.S., Shor G.G., LeRoy M. and Dorman J. 1981. Linear inversion of body wave data – Part II: Attenuation versus depth using spectral ratios. *Geophysics* 46, No. 2, 1520162.
- Jones I.F. 2010. *An Introduction to Velocity Model Building*. EAGE. ISBN 978-90-73781-84-9, 296 pages.
- Jones I.F., Sugrue M.J. and Hardy P.B. 2007. Hybrid Gridded Tomography. *First Break* 25, No. 4, 15–21.
- Liu H.-P., Anderson D.L. and Kanamori H. 1976. Velocity dispersion due to anelasticity; Implications for seismology and mantle composition. *Geophysical Journal of the Royal Astronomical Society* 47, Issue 1, 41–58.
- Mavko G. 2005. Parameters that Influence Seismic Velocity. <http://pangea.stanford.edu/courses/gp262/Notes/8.SeismicVelocity.pdf>
- Minshull T.A., Singh S.C. and Westbrook G.K. 1994. Seismic velocity structure at a gas hydrate reflector, offshore western Colombia, from full waveform inversion. *Journal of Geophysical Research* 99, 4715–4734.
- Reister D.B. 2003. Using Measured Velocity to Estimate Gas Hydrates Concentration. *Geophysics* 68, No. 3 (May–June 2003), 884–891.
- Riedel M., Willoughby E.C. and Chopra S. 2010. *Geophysical Characterization of Gas Hydrates*. SEG, ISBN 978-1-56080-218-1, 408 pages.
- Smith P., Jones I.F., King D.G., Sangvai P., Biswal A. and Mathur M. 2008. Deep Water Pre- Processing: East Coast India. *First Break* 26, No. 5, 101–107.
- Sun L.F. and Milkereit B. 2008. Seismic Velocity Dispersion and the Petrophysical Properties of Porous Media. Expanded Abstracts, CSPG CSEG CWLS Convention, p. 358–362.
- Sun L.F., Milkereit B. and Schmitt D.R. 2009. Measuring velocity dispersion and attenuation in the exploration seismic frequency band. *Geophysics* 74, No. 2, March–April, wa113–wa122.
- Walls J., Taner M.T., Mavko G. and Dvorkin J. 2002. Seismic Attenuation for Reservoir Characterization. US Dep. Energy quarterly report: DE-FC26-01BC15356, April.
- Werner H. and Krey T. 1979. Combisweep – A contribution to sweep techniques. *Geophysical Prospecting* 27, No. 1, 78–105.
- Zhang Y., Zhang P. and Zhang H. 2010. Compensating for viscoacoustic effects in reverse-time migration. *SEG Expanded Abstracts* 29, 3160.